Changes in Winter Atmospheric Rivers along the North American West Coast in CMIP5 Climate Models

MICHAEL D. WARNER AND CLIFFORD F. MASS

Department of Atmospheric Sciences, University of Washington, Seattle, Washington

ERIC P. SALATHÉ JR.

Science and Technology Program, University of Washington Bothell, Bothell, Washington

(Manuscript received 1 April 2014, in final form 5 August 2014)

ABSTRACT

Most extreme precipitation events that occur along the North American west coast are associated with winter atmospheric river (AR) events. Global climate models have sufficient resolution to simulate synoptic features associated with AR events, such as high values of vertically integrated water vapor transport (IVT) approaching the coast. From phase 5 of the Coupled Model Intercomparison Project (CMIP5), 10 simulations are used to identify changes in ARs impacting the west coast of North America between historical (1970–99) and end-of-century (2070–99) runs, using representative concentration pathway (RCP) 8.5. The most extreme ARs are identified in both time periods by the 99th percentile of IVT days along a north–south transect offshore of the coast. Integrated water vapor (IWV) and IVT are predicted to increase, while lower-tropospheric winds change little. Winter mean precipitation along the west coast increases by 11%–18% [from 4% to 6% $(°C)^{-1}$], while precipitation on extreme IVT days increases by 15%–39% [from 5% to 19% $(°C)^{-1}$]. The frequency of IVT days above the historical 99th percentile threshold increases as much as 290% by the end of this century.

1. Introduction

The U.S. West Coast receives the majority of its precipitation during the winter months (Neiman et al. 2008b), with the most extreme events associated with atmospheric rivers (ARs; Ralph et al. 2005, 2006; Dettinger et al. 2011; Warner et al. 2012). ARs are narrow regions of large water vapor transport that extend from the tropics or subtropics into the extratropics (Zhu and Newell 1998). ARs are responsible for over 90% of the global meridional water vapor transport but cover only a relatively small portion of the circumference of the globe at any time. ARs are crucial components of the hydrologic cycle in many parts of the world, including western North America (e.g., Dettinger 2004; Ralph et al. 2006, 2013; Neiman et al. 2011), western South America (Viale and Nunez 2011), and Europe (Sodemann and Stohl 2013; Lavers et al. 2013).

Global mean atmospheric water vapor is projected to increase with surface warming at roughly the rate of Clausius–Clapeyron scaling, about 7.5% $(°C)^{-1}$ (Held and Soden 2006; O'Gorman and Muller 2010). While global mean precipitation is expected to increase at a lesser rate, around 2%–3% $(°C)^{-1}$ (Trenberth 1999; Held and Soden 2006; O'Gorman and Muller 2010; Muller and O'Gorman 2011; O'Gorman et al. 2012; Stephens et al. 2012; Pendergrass and Hartmann 2014), extreme precipitation is predicted to increase at rates closer to that of global mean atmospheric water vapor (Allen and Ingram 2002; Trenberth et al. 2003; Pall et al. 2007). The above studies examined changes in mean and extreme precipitation on a global scale; it is unclear what changes can be expected on regional scales.

Extreme precipitation might also be influenced by dynamical changes associated with anthropogenic global warming (Groisman et al. 2005; Held and Soden 2006; Trenberth et al. 2007). It has been theorized that changes in equator-to-pole temperature gradient (Yin 2005) and Hadley cell expansion associated with global warming could shift the storm track poleward and/or upward in the

Corresponding author address: Michael Warner, Department of Atmospheric Sciences, University of Washington, Box 351640, Seattle, WA 98195-1640.
E-mail: mdwarner@atmos.washington.edu

DOI: 10.1175/JHM-D-14-0080.1

Northern Hemisphere (McCabe et al. 2001; Hu and Fu 2007; Lu et al. 2007; Meehl et al. 2007; Chang et al. 2012; Scheff and Frierson 2012; Singh and O'Gorman 2012; Barnes and Polvani 2013). Since ARs are typically located just south of the jet axis (Browning and Pardoe 1973; Neiman et al. 2008b; Cordeira et al. 2013), changes in the midlatitude jet stream could impact the location and frequency of ARs and extreme precipitation along the west coast (Salathé 2006; Mass et al. 2011; Dettinger 2011).

While numerous studies have addressed the origin, evolution, and coastal influence of ARs (e.g., McGuirk et al. 1987; Lackmann and Gyakum 1999; Ralph et al. 2004; Neiman et al. 2008a,b; Warner et al. 2012), relatively few have examined how projected changes in climate could impact AR location and intensity. One recent study (Dettinger 2011) evaluated seven Intergovernmental Panel on Climate Change (IPCC) Fourth Assessment Report (AR4) climate models, driven by the A2 scenario, for daily low-level integrated water vapor transport (IVT) at a single location off the central California coast. Examining both contemporary (1961–2000) and end-of-century (2081–2100) December–February periods, this study found that the winter AR season lengthens, the average intensity of the storms change little, and extreme storm intensities increase. Integrated water vapor (IWV) at that location increased in all the models, with low-level winds generally decreasing. Lavers et al. (2013) used phase 5 of the Coupled Model Intercomparison Project (CMIP5) output from five climate models in the IPCC Fifth Assessment Report (AR5; Taylor et al. 2012) to identify changes in ARs at the end of the twenty-first century (2074–99) over the eastern Atlantic Ocean and the United Kingdom. They found the changes in ARs were driven by increases in atmospheric water vapor due to warming, with a doubling in AR frequency and increases in heavy precipitation by the end of this century.

Regional precipitation frequency and intensity can be poorly represented by global climate models (GCMs) because of inadequate resolution, among other causes (Stephens et al. 2010; Flato et al. 2013, section 9.4). While significant issues like errors in cyclone intensity (Colle et al. 2013; Zappa et al. 2013) and storm-track location (Chang et al. 2012) still exist, GCM-simulated large-scale storm tracks in the extratropics continue to improve (Flato et al. 2013, section 9.4.1.4.3), at least in part through increases in horizontal resolution (Colle et al. 2013). With improving GCM fidelity on the synoptic scale, west coast AR events can be identified by high values of IVT (Neiman et al. 2008b). Utilizing state-of-the-art CMIP5 climate models and using representative concentration pathway (RCP) 8.5[1] over the eastern Pacific, this study identifies extreme IVT events along the U.S. West Coast, quantifies the changes in IVT and precipitation due to increasing anthropogenic greenhouse gases, and identifies what portion of these changes are due to modifications of wind and IWV.

2. Data and methods

GCMs are not ideal tools for studying extreme precipitation impacting the west coast because of their relatively coarse horizontal grid spacing and poor representation of coastal terrain (Widmann et al. 2003; Stephens et al. 2010). However, ARs can be identified by associated synoptic-scale features resolved by coarse-resolution GCMs, such as synoptic-scale IWV or IVT plumes intersecting the coast. The IPCC CMIP5 archive offers an opportunity to identify AR events in both contemporary and future simulations for a range of global warming scenarios.

Since AR-associated extreme precipitation generally lasts for about one day along the west coast (Ralph et al. 2013; Rutz et al. 2014), daily mean values are used in this analysis. Surface temperature, specific humidity, u- and v-wind components (zonal and meridional, respectively), and total daily precipitation were retrieved from the Program for Climate Model Diagnosis and Intercomparison (PCMDI) website (http://pcmdi9.llnl.gov/esgf-web-fe/). To compare two 30-yr periods separated by 100 years: 1970–99 and 2070–99, 10 CMIP5 historical and RCP 8.5 models were used (Table 1). Models without surface winds or surface specific humidity available were not considered, since these fields are necessary for calculating IWV and IVT using the method described below. Models with a longitudinal grid spacing of greater than 2.5° were eliminated to avoid land-fraction contamination for analysis points immediately off the coast (Fig. 1). RCP 8.5 was chosen because it is widely believed to be the most realistic scenario for "business as usual" carbon dioxide emissions (Meehl et al. 2012; Bopp et al. 2013). Some models were represented by more than one ensemble member. Thus, to eliminate favoring a specific model in the results, only the first ensemble member for each model was used. Model output was regridded to a common grid of 1.25° × 1.875°, similar to that of the Hadley Centre Global Environment Model, version 2.

Several studies have shown that IVT has a close relationship with the amount of orographically produced precipitation along the west coast (Neiman et al. 2002; Ralph et al. 2006; Neiman et al. 2008b; Viale and Nunez 2011; Ralph et al. 2013); thus, IVT is examined in this study. For each model, extreme IVT days were identified at a line of grid points located off the U.S. West Coast (Fig. 1) by finding the 99th percentile in daily IVT

[1] An 8.5 W m^{-2} increase in total radiative forcing by the year 2100.

TABLE 1. CMIP5 historical (1970–99) and RCP 8.5 (2070–99) models used and associated horizontal resolution.

Model	Original resolution		Modeling center
	Lat (°)	Lon (°)	
MRI-CGCM3 (Meteorological Research Institute Coupled Atmosphere–Ocean General Circulation Model, version 3)	1.1215	1.1250	Meteorological Research Institute (Japan)
Model for Interdisciplinary Research on Climate, version 5 (MIROC5)	1.4000	1.4062	Model for Interdisciplinary Research on Climate (Japan)
Centre National de Recherches Météorologiques Coupled Global Climate Model, version 5 (CNRM-CM5)	1.4000	1.4062	Centre National de Recherches Météorologiques (France)
Hadley Centre Global Environment Model, version 2–Carbon Cycle (HadGEM2-CC)	1.2500	1.8750	Met Office Hadley Centre (United Kingdom)
Commonwealth Scientific and Industrial Research Organisation Mark 3.6.0 (CSIRO Mk 3.6.0)	1.8650	1.8750	Commonwealth Scientific and Industrial Research Organisation (Australia)
Institute of Numerical Mathematics Coupled Model, version 4.0 (INM-CM4.0)	1.5000	2.0000	Institute of Numerical Mathematics (Russia)
L'Institut Pierre-Simon Laplace Coupled Model, version 5, coupled with the Nucleus for European Modelling of the Ocean (NEMO), mid resolution (IPSL-CM5A-MR)	1.2676	2.5000	L'Institut Pierre-Simon Laplace (France)
Geophysical Fluid Dynamics Laboratory Climate Model, version 3 (GFDL-CM3)	2.0000	2.5000	Geophysical Fluid Dynamics Laboratory (United States)
Geophysical Fluid Dynamics Laboratory Earth System Model with Generalized Ocean Layer Dynamics (GOLD) component (GFDL-ESM2G)	2.0225	2.5000	Geophysical Fluid Dynamics Laboratory (United States)
Geophysical Fluid Dynamics Laboratory Earth System Model with Modular Ocean Model 4 (MOM4) component (GFDL-ESM2M)	2.0225	2.5000	Geophysical Fluid Dynamics Laboratory (United States)

during winter (October–March) for the 30-yr historical and future periods at each point. The full wind speed was used in the IVT calculation; large IVT values are inevitably associated with winds from the south to west. Because the majority of water vapor transport (~75%) occurs in the lowest 2.5 km of the atmosphere (Ralph et al. 2005) and previous studies used lower levels to define IVT (Neiman et al. 2008b; Moore et al. 2012), this study defines IVT ($\mathrm{kg\,m^{-1}\,s^{-1}}$) using total wind speed and specific humidity at the surface and at 850-, 700-, and 500-hPa levels[2]:

$$\mathrm{IVT} = \frac{1}{g_0}\int_{\mathrm{sfc}}^{500} \overline{q}\,\overline{U}\,dp, \qquad (1)$$

where $\overline{q}$ is mean layer specific humidity ($\mathrm{kg\,kg^{-1}}$), $\overline{U}$ is mean layer total wind ($\mathrm{m\,s^{-1}}$), g_0 is acceleration due to gravity ($\mathrm{m\,s^{-2}}$), and dp is the difference in pressure between layers (hPa). The 99th percentile days in IVT are hereafter referred to as "extreme days." In addition, 30-yr averages of IVT were calculated for the winter season (hereafter referred to as winter average) of both time periods. For verification, IVT was also calculated using the National Centers for Environmental Prediction–National Center for Atmospheric Research (NCEP–NCAR) reanalysis (Kalnay et al. 1996) for the historical period.[3]

For extreme days and the winter average, IVT was broken down into its two components, IWV and wind. Additionally, precipitation on 99th percentile IVT days is examined to identify possible changes in precipitation intensity. The precipitation is analyzed offshore in the same location as IVT to minimize any possible effects of orographic enhancement in the analysis. The Student's t statistic was used to determine if the end-of-century (2070–99) multimodel mean is statistically different from the historical (1970–99) multimodel mean for both the winter averages and the extreme days for IVT, IWV, low-level wind, and precipitation.

Finally, to assess changes in frequency in extreme precipitation, an event threshold was set at each grid

[2] The 1000-hPa level of the atmosphere is not considered in IWV or IVT calculations because of lack of data at this level or at the surface in each of the included models over large areas of the ocean where surface pressures are below 1000 hPa.

[3] The NCEP–NCAR reanalysis for the period 1970–99 used in this analysis spans the beginning of the satellite era (starting in roughly 1979), and the quality of the reanalysis likely improved in time. At least one study found the NCEP–NCAR reanalysis precipitable water and precipitation to have only small differences with observations in the eastern North Pacific Ocean (Trenberth and Guillemot 1998) from 1988 to 1992, a period in which satellite observations were being assimilated into the reanalysis.

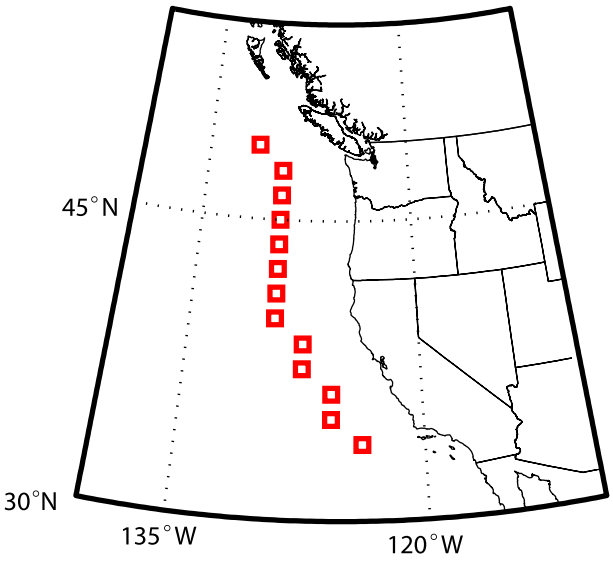

FIG. 1. Locations evaluated in CMIP5 models and reanalysis grids.

point in Fig. 1: the lowest value to reach the 99th percentile of IVT during the historical period. The number of days in the end-of-twenty-first-century period to reach this IVT threshold was used to calculate the percent increase in days with extreme IVT and thus, implicitly, extreme precipitation.

3. Results

Figures 2a and 2b show multimodel mean and individual model results of IVT for the winter average and extreme days for 1970–99 (Fig. 2a) and 2070–99 (Fig. 2b) for 13 points along the transect shown in Fig. 1. IVT from the NCEP–NCAR reanalysis is also shown for 1970–99 (Fig. 2a) for reference. For both the winter average and the extreme days during the historical period, the NCEP–NCAR reanalysis IVT closely matches the multimodel mean. At all points, the historical mean 99th percentile IVT is much greater than 250 kg m^{-1} s^{-1}, the threshold flux used to identify ARs in some previous literature (Moore et al. 2012; Cordeira et al. 2013; Rutz et al. 2014). There is an increase in 99th percentile IVT by 26%–30% between historical and future periods at all points. There is little overlap between the model ranges of IVT in the historical and future runs, and the extreme days in the end-of-century simulation generally fall outside of the historical model range. During both the historical and late-twenty-first-century periods, the peak IVT for both ensemble-mean extreme days and the winter average are found in the middle latitudes of the domain, for reasons discussed later. The multimodel means between the historical and future periods for both winter average and the extreme days are statistically different at the 95% confidence level for all points along the transect.

Once the 99th percentile days are chosen using IVT, the individual components of IVT during the selected days, the IWV and the low-level wind, were evaluated separately. Figures 2c and 2d show IWV for multimodel means and individual models for the winter average and extreme days for both historical and future conditions. The NCEP–NCAR reanalysis closely matches the historical multimodel mean for extreme days; however, the NCEP–NCAR reanalysis shows higher values of IWV than the multimodel winter average at all points, with a greater difference to the north, but remains within the model range. During both periods, the observed and model IWV show a decrease from south to north for both the extreme days and the winter average. This is consistent with the proximity of the southern part of the domain to larger IWV values in the tropics. For the extreme days, there is very little overlap in model ranges between historical and future simulations of IWV, with minor overlap of model ranges for the winter average. In the case of the extremes, all IWV values greatly exceed 2 cm, the threshold for AR events described in previous literature (Ralph et al. 2004). The changes from historical to end-of-twenty-first-century periods in the multimodel mean in IWV for both the winter average and the extreme days are statistically significant at the 95% level for all points along the transect.

While high IWV values are an important aspect of AR events, large IVT values also rely on strong low-level winds for advecting moist air toward the coast, forcing ascent over coastal terrain and leading to orographic precipitation. Figures 2e and 2f show multimodel means and individual models of 850-hPa total wind for the winter average and during the IVT extremes for both the historical and future climates. The 850-hPa wind was chosen because that level typically intersects the upper slopes of major western U.S. terrain barriers. The NCEP–NCAR reanalysis 850-hPa wind closely matches the multimodel mean for the extreme days over the far southern and northern portions of the transect but is near the high end of the model range for the middle latitudes (~44°N). Additionally, the 99th percentile 850-hPa wind along the transect (20–25 m s^{-1}) closely matches aircraft observed winds under AR conditions analyzed previously in Ralph et al. (2005). In the multimodel winter averages, there is a fairly steady increase in 850-hPa wind from south to north and a close correspondence with reanalysis values. Such a meridional increase is consistent with the typical location of the midlatitude jet stream over the northern portion of the domain from October through March. It appears that the peak in extreme IVT over the midcoast (northern California)

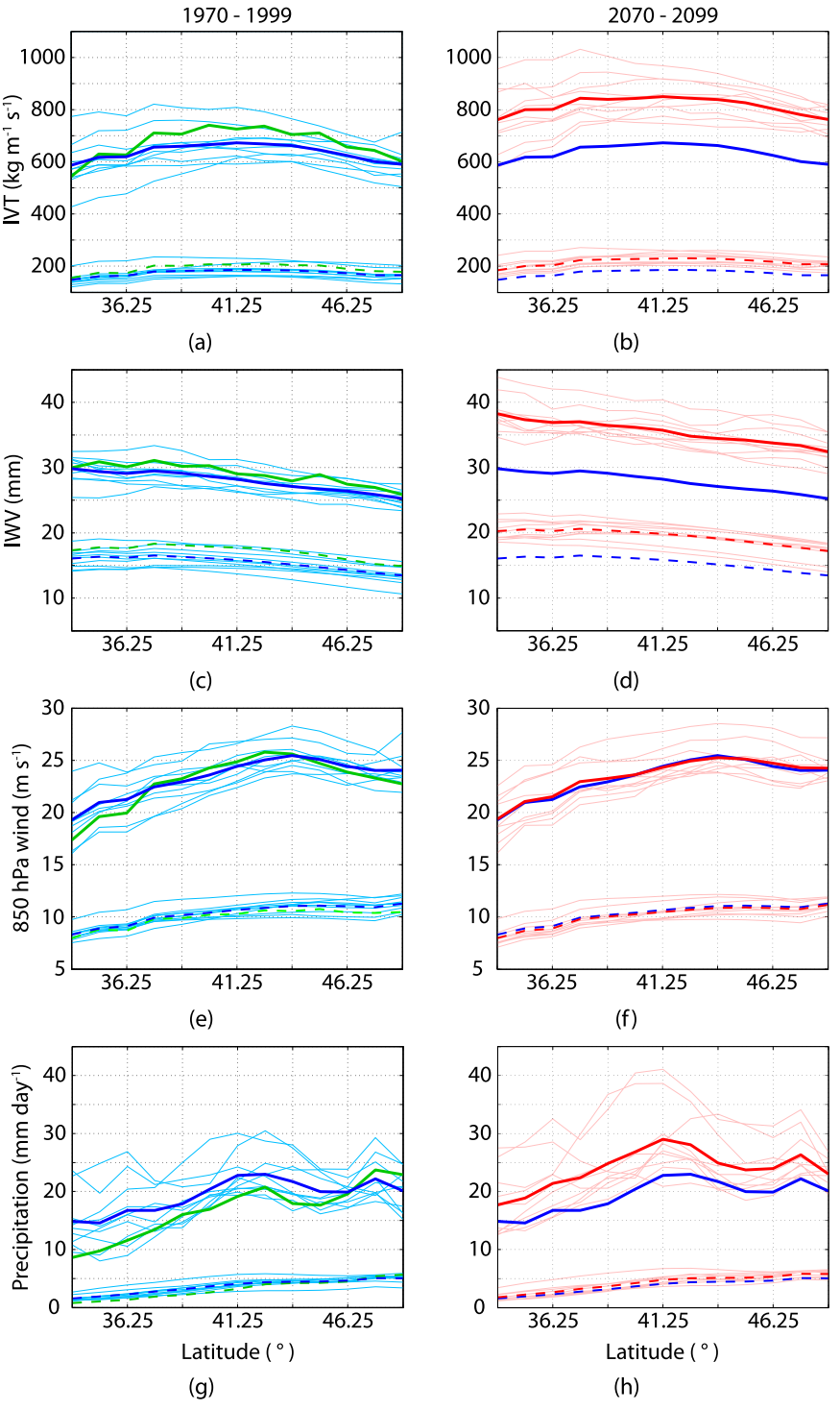

FIG. 2. CMIP5 RCP 8.5 10-model means (boldface lines) for (a),(b) 99th percentile IVT (upper values, solid) and winter mean (lower values, dashed) for (left) 1970–99 (boldface blue) and (right) 2070–99 (boldface red) along the 13-grid-box transect in Fig. 1. Only October–March is considered. Light blue and red lines are individual models, and boldface green lines on the left are NCEP–NCAR reanalysis values for 1970–99. Right-hand plots also show the multimodel means of the historic period for reference (boldface blue lines, same on left and right). Similar plots for (c),(d) IWV; (e),(f) 850-hPa total wind; and (g),(h) daily precipitation are also shown.

for both the historical and future periods can be explained by the conflation of the decreasing IWV to the north and the general increase of lower-tropospheric winds to the north, with their product maximizing in the middle of the domain. The models predict very little change in 850-hPa wind along the west coast between the historical and future periods for either the winter average or the extreme days, and none of the changes are statistically significant anywhere along the transect. Similarly, very little change in winter-average wind or wind on extreme days were observed at other levels up to 500-hPa (not shown).

Figures 2g and 2h show the multimodel mean and individual model values of daily precipitation[4] for winter average and extreme days for both the historical and end-of-century simulation periods. For both the winter averages and extreme days during the historical period, the multimodel mean modestly overestimates precipitation south of approximately 46°N, although the NCEP–NCAR reanalysis precipitation is generally contained within the model envelope. There is a modest precipitation increase from south to north for the model winter average. Historical extreme precipitation shows more meridional modulation, with a broad secondary peak near 41°N and a narrow primary peak over the far northern portion of the domain. It is possible that the northern peak is a result of the westward curving coastline of British Columbia and the proximity of terrain to the meridional transect. The future simulation has more precipitation along the transect than the historical climate for both the winter average and extreme days, although the model range is quite large and there is considerable overlap between historical and future runs.

On extreme days, absolute increases between the historical and future periods are largest (roughly 5 mm day^{-1}) from approximately 36° to 40°N (Fig. 2h); percent change ranges from roughly 35% for 36°–40°N, with considerable model spread, to about 19% north of 40°N, with relatively less model spread (Fig. 3a). The absolute difference in the extreme precipitation between the historical and end-of-century periods is statistically significant at the 95% confidence level for all but 3 out of 13 points along the transect (33.75°, 47.50°, and 48.75°N), in contrast to the differences in winter-average precipitation, which are statistically significant at the 95% confidence level at only the four northernmost points (45.00°–48.75°N).

While change in surface air temperature between the historical and late-twenty-first-century periods are similar (~3°C) for winter averages and extreme days over the

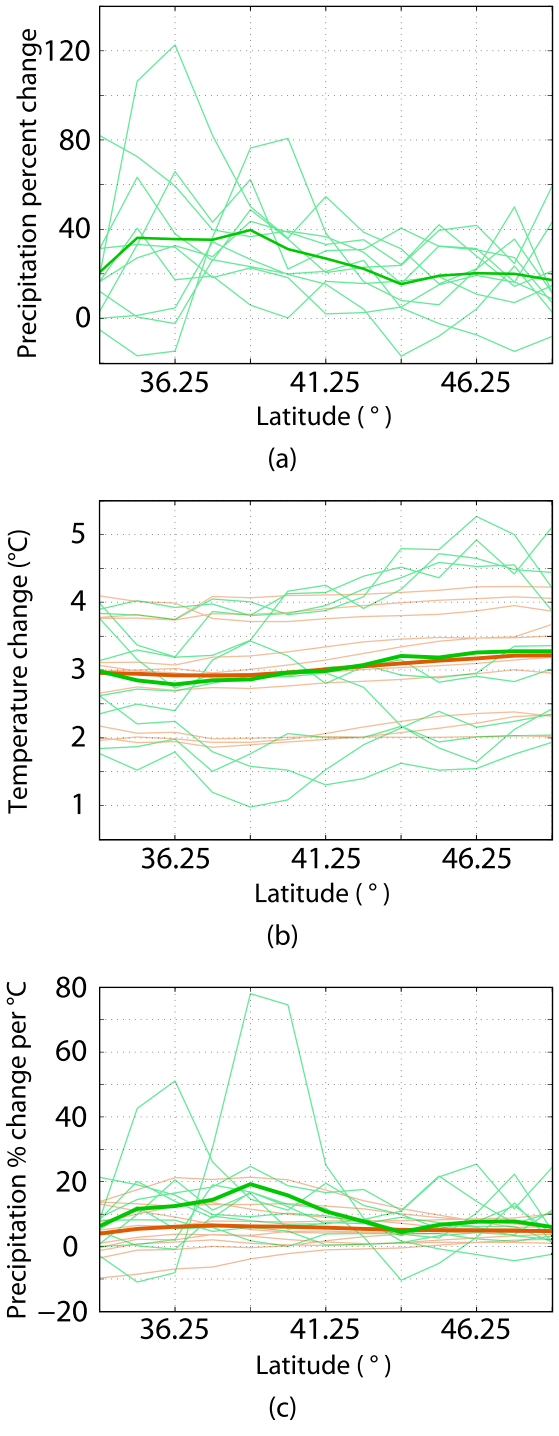

FIG. 3. (a) CMIP5 RCP 8.5 10-model-mean percent change in precipitation from 1970–99 to 2070–99 for the 99th percentile events in IVT (boldface green). (b) Similar mean surface temperature change from 1970–99 to 2070–99 for the winter mean (boldface brown) and 99th percentile events in IVT (boldface green). (c) The corresponding percent change in precipitation per degree Celsius of surface warming at the transect locations for winter mean (boldface brown) and 99th percentile events in IVT (boldface green). Light green or brown lines are individual models comprising the mean.

[4] CMIP5 models provide precipitation as a surface flux. Here, precipitation flux (kg m^{-2} s^{-1}) has been converted to daily precipitation (mm day^{-1}).

entire domain (Fig. 3b), there are substantial differences for winter-average and extreme precipitation changes per degree Celsius of warming: 4%–6% $(°C)^{-1}$ increases in winter-average precipitation versus 5%–19% $(°C)^{-1}$ increases in precipitation for extreme days (Fig. 3c). Although there is no reason to expect regional changes in precipitation per degree Celsius to match globally averaged values [~2%–3% $(°C)^{-1}$ for means, ~7.5% $(°C)^{-1}$ for extremes], percent changes in precipitation per degree Celsius of warming along this transect are only slightly higher than expected globally (Held and Soden 2006; O'Gorman and Muller 2010). While the sensitivity of winter-average precipitation with respect to temperature is nearly constant with latitude [4%–6% $(°C)^{-1}$] in the present study, the temperature sensitivity for extreme precipitation is higher [7%–19% $(°C)^{-1}$] over the southern portion of the domain (36°–40°N) with large model variability. For both the winter average and the extreme days, there is larger model spread over the southern portion of the transect than farther north.

Why is extreme precipitation more sensitive to temperature from approximately 36° to 40°N? First, the percentage change in precipitation is largest in that band (Fig. 3a). Second, the temperature change associated with extreme precipitation is smallest over the southern portion of the domain (Fig. 3b). Larger change in precipitation for a smaller variation in temperature produces enhanced sensitivity. Possible reasons for the reduced temperature change in the atmospheric river are discussed in the final section.

At all points along the coastal transect, there are end-of-century increases in the number of days with extreme precipitation based on the 99th percentile threshold of IVT for 1970–99 (Table 2). Although multimodel-mean winter-average and extreme IVT increase by about 25%–30% (Fig. 2b), there are 230%–290% increases in the number of days above the historical threshold, with a modest peak around 45°N (Table 2).

As shown in Fig. 4a, while there is a large increase in the number of days with high values of IVT for 2070–99, there is also a significant decrease in days with lower values of IVT, because the area under both curves are the same (same number of days in both time periods). Dettinger (2011) noted similar behavior in model IVT at a point off the central California coast, while Allen and Ingram (2002) found analogous results for globally averaged model precipitation. As illustrated here using the mean 99th percentile IVT threshold for the historical period (559 $kg\,m^{-1}\,s^{-1}$), the changes in the highly skewed IVT distributions can produce large changes in the frequency of extreme IVT days.

Table 2 suggests a larger increase in the number of extreme IVT days north of 41.25°N than south of that latitude. Because there is little change in wind along the transect during the two periods (Fig. 2f) and the IVT does not increase more to the north, this implies that there is a difference of the histograms of IVT so that a shift to a moister/warmer climate pushes above a fixed threshold more to the north. This is demonstrated in Fig. 4b, which shows the winter distributions of IVT for the north and south portions of the transect for both historical and future periods. The north has a higher frequency than the south of intermediate IVT (300–500 $kg\,m^{-1}\,s^{-1}$) during the historical period, and thus increases in water vapor associated with warming will tend to push the northern sections above a fixed threshold more than locations to the south.

TABLE 2. Multimodel means by lat of historical (1970–99) IVT 99% thresholds, number of days above the historical threshold in RCP 8.5 simulation for 2070–99, and the percent increase over the historical in number of days over threshold for 2070–99. The third and fourth columns have been rounded to the nearest integer. The mean number of days above the threshold for the historical period is 55.

Lat (°N)	Mean historical threshold ($kg\,m^{-1}\,s^{-1}$)	Mean days above historical threshold for 2070–99	Mean increase (%) over historical threshold
48.75	524.08	215	291
47.50	521.40	209	280
46.25	551.51	206	275
45.00	566.58	211	285
43.75	579.32	210	283
42.50	591.06	198	260
41.25	597.17	180	228
40.00	586.97	185	236
38.75	578.60	186	239
37.50	577.99	183	234
36.25	540.99	182	231
35.00	534.76	182	232
33.75	499.60	179	227

4. Discussion and conclusions

CMIP5 climate simulations suggest significant increases in integrated water vapor transport (IVT) along the North American west coast as anthropogenic greenhouse gases increase during the coming century. Because coastal precipitation over the western United States is greatly enhanced by the interaction of incoming IVT with regional terrain (Ralph et al. 2006; Neiman et al. 2008b; Viale and Nunez 2011), both winter-average and extreme precipitation are expected to increase in this region if IVT increases. The CMIP5 simulations considered in this study indicate that an increase in IVT and associated precipitation between historical (1970–99) and future (2070–99) periods will be due to large simulated increases in integrated water vapor (IWV)

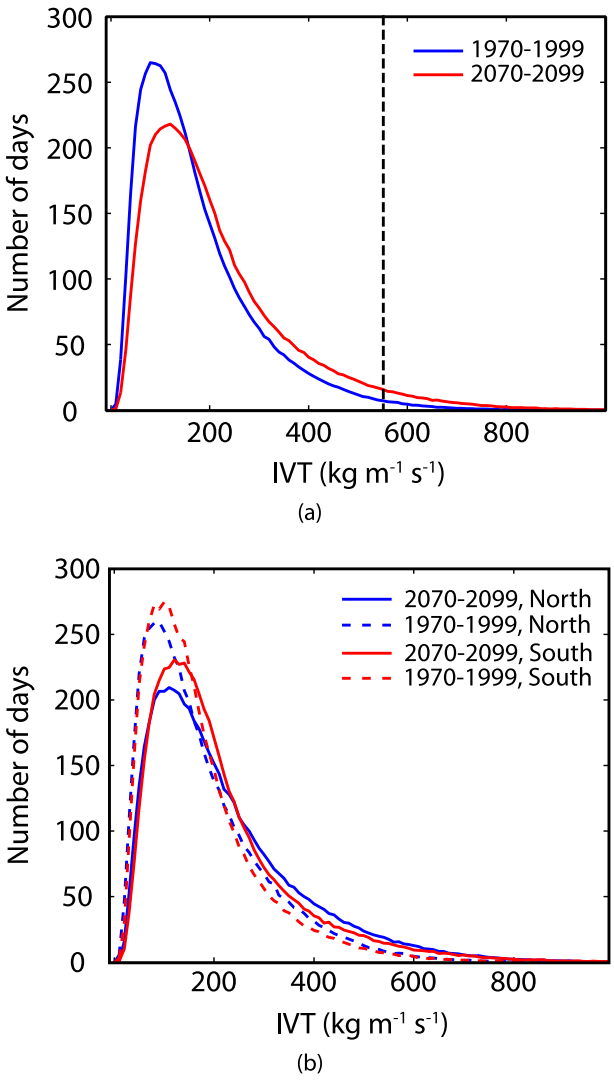

FIG. 4. (a) Multimodel cool season–mean (October–March) IVT distributions of the number of days with varying IVT amounts for 1970–99 (blue) and 2070–99 (red) for all points of the north–south transect. Black dotted line indicates mean historical 99th percentile threshold (559 kg m^{-1} s^{-1}) for IVT days. (b) Multimodel cool season–mean IVT distributions for the six northern points for 1970–99 (blue dashed) and 2070–99 (blue solid) and the six southern points for 1970–99 (red dashed) and 2070–99 (red solid). For (a) and (b), 150 equally sized IVT bins were used, and there is equal area under all curves. Curves extend to roughly 1500 kg m^{-1} s^{-1} but are cropped at 1000 kg m^{-1} s^{-1} to show detail.

and not changes in low-level wind speed, consistent with the Dettinger (2011) analysis at one point near the central California coast and the Lavers et al. (2013) analysis in the North Atlantic and the United Kingdom. Specifically, increases in winter-average and extreme precipitation along the offshore transect in the present study were found to be 11%–18% and 15%–39%, respectively. The sensitivities of precipitation changes to warming along the west coast were found to be 4%–6% (°C)$^{-1}$ for winter averages and 5%–19% (°C)$^{-1}$ for the top 1% events, both higher than expected for the global mean [~2%–3% (°C)$^{-1}$ for means, ~7.5% (°C)$^{-1}$ for extremes]. To put these results into context, various studies have found differing extents of precipitation change per degree Celsius warming depending on spatial and temporal scales. For instance, O'Gorman and Schneider (2009) found that changes per degree Celsius of warming of extreme precipitation in the midlatitudes were less than changes in IWV values per degree Celsius warming. Conversely, Lenderink and van Meijgaard (2010) found increases in hourly extreme precipitation were double that expected from Clausius–Clapeyron. In the case of extremes related to ARs in the eastern North Pacific and west coast region, Dettinger (2011) found that the frequency of average AR conditions does not change much but that the most extreme events change substantially. Given that the present study is sampling the most extreme events, ones with IVT values well above thresholds defined in previous studies (e.g., Rutz et al. 2014), the results here are consistent with Dettinger (2011). Furthermore, the large frequency increases of IVT days above historical thresholds found in the present study are consistent with Lavers et al. (2013) in the United Kingdom, where they noted a doubling of AR events by the end of the century.

Higher than global-average sensitivity of precipitation to warming might be partially explained by the importance of atmospheric rivers (ARs) along the west coast. As shown in Fig. 5, temperature change between historical and future periods is minimized over the climatological-mean location of the AR compared to adjacent regions. Extreme precipitation in the midlatitudes is often related to air masses that have traveled from places farther south (O'Gorman and Schneider 2009), where temperature is projected to change less rapidly than farther north under global warming (van Oldenborgh et al. 2013, Fig. AI.SM8.5.4). Although much of the IWV in the column is converged from local sources during AR events (e.g., Bao et al. 2006), at least some of the IWV has origins nearer the tropics (Sodemann and Stohl 2013); thus, the temperature change in the AR core is more similar to locations farther south. Another explanation for less temperature change (from historical to future) in the core of the AR composite mean could be because of changes in lapse rates. At 500 hPa (not shown), the southeast–northwest horizontal temperature change gradient is greatly reduced compared to the surface, and the signature of less temperature change in the core of the AR is not seen like at the surface (Fig. 5). Because the AR core (where relative humidities are very near 100% in the boundary layer) follows a more or less moist adiabatic lapse rate to the surface (Ralph et al.

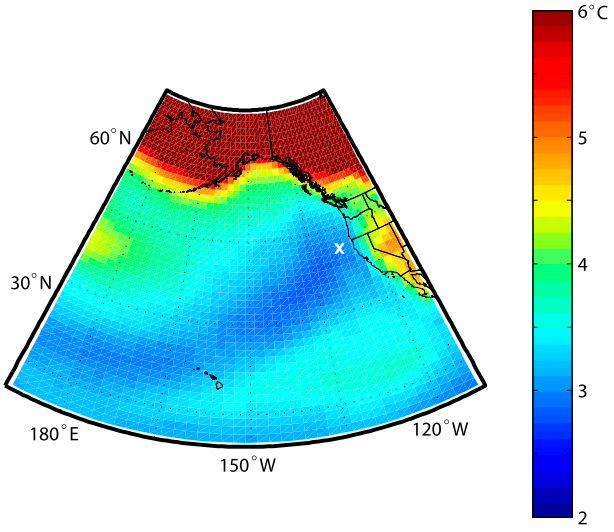

FIG. 5. Multimodel-mean surface air temperature change (°C) during AR days at 41.25°N (white cross) from 1970–99 to 2070–99. AR days are defined as the 99th percentile IVT days, so the same number of days are used in each of the time periods.

2005), the temperature in this area is expected to be cooler than areas where the lapse rate is between moist and dry adiabatic, leading to a lesser surface temperature change in the core of the AR than outside of it.

The results along the transect used in this study show that the highest IVT values are found along the northern California and Oregon coasts (Figs. 1, 2). Temperature slowly decreases from south to north, while the distance to the tropical source region of high concentrations of water vapor decreases. Thus, the IWV content declines to the north. On the other hand, there are higher wind speeds to the north, closer to the location of the climatological jet stream. The conflation of the two opposite latitudinal trends results in a broad maximum in IVT near the middle of the transect (38°–44°N).

Precipitation extremes peak near the middle of the transect, with a secondary maximum over the northern extreme of the domain (Figs. 2g,h). If IVT is a proxy for coastal precipitation, one might expect a maximum in precipitation in the middle of the transect. The northern peak in extreme precipitation may be explained by the sharp westward turn of terrain near the U.S./Canada border, which allows coastal uplift to impact the northern transect points. Winter-mean precipitation steadily increases to the north, consistent with the larger number of weak to moderate systems over the northern portion of the domain.

Several studies suggest a poleward shift of subtropical and midlatitude jet streams due to anthropogenic climate change (Hu and Fu 2007; Lu et al. 2007; Chang et al. 2012; Barnes and Polvani 2013). Because ARs generally are found immediately south of the jet stream and its associated frontal boundary, a northern shift of the climatological jet stream would tend to lessen AR frequencies to the south and increase them to the north. However, as shown in Fig. 2f, there is little suggestion of a latitudinal shift in the low-level portion of the jet stream over the west coast during the next century. This is consistent with Barnes and Polvani (2013), which found that spatial shifts in the Pacific eddy-driven jet stream are small. Thus, the main impact of global warming on heavy precipitation along the west coast of North America appears to be the enhancement of the water vapor content of the approaching air, a result that is consistent with Dettinger (2011) and studies done in the Atlantic Ocean and Europe (Lavers et al. 2013).

As noted earlier, precipitation is greatly enhanced as ARs intersect the coastal terrain, but it is uncertain how global warming will alter orographic enhancement. CMIP5 RCP 8.5 simulations indicate low-level moisture and IVT will be increasing significantly, but changes may also occur in tropospheric stability (Frierson 2006) and wind shear (Lu et al. 2007; Chang et al. 2012), important factors in modulating both the amount of orographically induced precipitation and its spatial distribution (Kirshbaum and Durran 2004; Colle 2004). For a more thorough understanding of global warming–induced precipitation changes along west coast terrain, future work will evaluate regionally dynamically downscaled models on days where ARs are approaching the coast.

Acknowledgments. This research was supported by National Science Foundation Grant AGS-1041879. The authors thank Dr. Dargan Frierson and Dr. Jack Scheff for thoughtful discussions and three anonymous reviewers who provided valuable feedback that greatly improved this manuscript.

REFERENCES

Allen, M. R., and W. J. Ingram, 2002: Constraints on future changes in climate and the hydrologic cycle. *Nature,* **419,** 224–232, doi:10.1038/nature01092.

Bao, J.-W., S. A. Michelson, P. J. Neiman, F. M. Ralph, and J. M. Wilczak, 2006: Interpretation of enhanced integrated water vapor bands associated with extratropical cyclones: Their formation and connection to tropical moisture. *Mon. Wea. Rev.,* **134,** 1063–1080, doi:10.1175/MWR3123.1.

Barnes, E. A., and L. Polvani, 2013: Response of the midlatitude jets, and of their variability, to increased greenhouse gases in the CMIP5 models. *J. Climate,* **26,** 7117–7135, doi:10.1175/JCLI-D-12-00536.1.

Bopp, L., and Coauthors, 2013: Multiple stressors of ocean ecosystems in the 21st century: Projections with CMIP5 models. *Biogeosciences,* **10,** 6225–6245, doi:10.5194/bg-10-6225-2013.

Browning, K. A., and C. W. Pardoe, 1973: Structure of low-level jet streams ahead of mid-latitude cold fronts. *Quart. J. Roy. Meteor. Soc.,* **99,** 619–638, doi:10.1002/qj.49709942204.

Chang, E. K. M., Y. Guo, and X. Xia, 2012: CMIP5 multimodel ensemble projection of storm track change under global warming. *J. Geophys. Res.,* **117,** D23118, doi:10.1029/2012JD018578.

Colle, B. A., 2004: Sensitivity of orographic precipitation to changing ambient conditions and terrain geometries: An idealized modeling perspective. *J. Atmos. Sci.,* **61,** 588–606, doi:10.1175/1520-0469(2004)061<0588:SOOPTC>2.0.CO;2.

——, Z. Zhang, K. A. Lombardo, E. Chang, P. Liu, and M. Zhang, 2013: Historical evaluation and future prediction of eastern North American and western Atlantic extratropical cyclones in the CMIP5 models during the cool season. *J. Climate,* **26,** 6882–6903, doi:10.1175/JCLI-D-12-00498.1.

Cordeira, J. M., F. M. Ralph, and B. J. Moore, 2013: The development and evolution of two atmospheric rivers in proximity to western North Pacific tropical cyclones in October 2010. *Mon. Wea. Rev.,* **141,** 4234–4255, doi:10.1175/MWR-D-13-00019.1.

Dettinger, M. D., 2004: Fifty-two years of "pineapple express" storms across the west coast of North America. California Energy Commission Doc. CEC-500-2005-004/California Climate Change Center Rep. 2005-003, 15 pp. [Available online at www.energy.ca.gov/2005publications/CEC-500-2005-004/CEC-500-2005-004.PDF.]

——, 2011: Climate change, atmospheric rivers, and floods in California—A multimodel analysis of storm frequency and magnitude changes. *J. Amer. Water Resour. Assoc.,* **47,** 514–523, doi:10.1111/j.1752-1688.2011.00546.x.

——, F. M. Ralph, T. Das, P. J. Neiman, and D. R. Cayan, 2011: Atmospheric rivers, floods and the water resources of California. *Water,* **3,** 445–478, doi:10.3390/w3020445.

Flato, G., and Coauthors, 2013: Evaluation of climate models. *Climate Change 2013: The Physical Science Basis,* T. F. Stocker et al., Eds., Cambridge University Press, 741–866.

Frierson, D. M. W., 2006: Robust increases in midlatitude static stability in simulations of global warming. *Geophys. Res. Lett.,* **33,** L24816, doi:10.1029/2006GL027504.

Groisman, P. Y., R. W. Knight, D. R. Easterling, T. R. Karl, G. C. Hegerl, and V. N. Razuvaev, 2005: Trends in intense precipitation in the climate record. *J. Climate,* **18,** 1326–1350, doi:10.1175/JCLI3339.1.

Held, I. M., and B. J. Soden, 2006: Robust responses of the hydrological cycle to global warming. *J. Climate,* **19,** 5686–5699, doi:10.1175/JCLI3990.1.

Hu, Y., and Q. Fu, 2007: Observed poleward expansion of the Hadley circulation since 1979. *Atmos. Chem. Phys.,* **7,** 5229–5236, doi:10.5194/acp-7-5229-2007.

Kalnay, E., and Coauthors, 1996: The NCEP/NCAR 40-Year Reanalysis Project. *Bull. Amer. Meteor. Soc.,* **77,** 437–471, doi:10.1175/1520-0477(1996)077<0437:TNYRP>2.0.CO;2.

Kirshbaum, D. J., and D. R. Durran, 2004: Factors governing cellular convection in orographic precipitation. *J. Atmos. Sci.,* **61,** 682–698, doi:10.1175/1520-0469(2004)061<0682:FGCCIO>2.0.CO;2.

Lackmann, G. M., and J. R. Gyakum, 1999: Heavy cold-season precipitation in the northwestern United States: Synoptic climatology and an analysis of the flood of 18 January 1986. *Wea. Forecasting,* **14,** 687–700, doi:10.1175/1520-0434(1999)014<0687:HCSPIT>2.0.CO;2.

Lavers, D. A., R. P. Allan, G. Villarini, B. Lloyd-Hughes, D. J. Brayshaw, and A. J. Wade, 2013: Future changes in atmospheric rivers and their implications for winter flooding in Britain. *Environ. Res. Lett.,* **8,** 034010, doi:10.1088/1748-9326/8/3/034010.

Lenderink, G., and E. van Meijgaard, 2010: Linking increases in hourly precipitation extremes to atmospheric temperature and moisture changes. *Environ. Res. Lett.,* **5,** 025208, doi:10.1088/1748-9326/5/2/025208.

Lu, J., G. A. Vecchi, and T. Reichler, 2007: Expansion of the Hadley Cell under global warming. *Geophys. Res. Lett.,* **34,** L06805, doi:10.1029/2006GL028443.

Mass, C., A. Skalenakis, and M. Warner, 2011: Extreme precipitation over the west coast of North America: Is there a trend? *J. Hydrometeor.,* **12,** 310–318, doi:10.1175/2010JHM1341.1.

McCabe, G. J., M. P. Clark, and M. C. Serreze, 2001: Trends in Northern Hemisphere surface cyclone frequency and intensity. *J. Climate,* **14,** 2763–2768, doi:10.1175/1520-0442(2001)014<2763:TINHSC>2.0.CO;2.

McGuirk, J. P., A. H. Thompson, and N. R. Smith, 1987: Moisture bursts over the tropical Pacific Ocean. *Mon. Wea. Rev.,* **115,** 787–798, doi:10.1175/1520-0493(1987)115<0787:MBOTTP>2.0.CO;2.

Meehl, G. A., and Coauthors, 2007: Global climate projections. *Climate Change 2007: The Physical Science Basis,* S. Solomon et al., Eds., Cambridge University Press, 747–845.

——, and Coauthors, 2012: Climate system response to external forcings and climate change projections in CCSM4. *J. Climate,* **25,** 3661–3683, doi:10.1175/JCLI-D-11-00240.1.

Moore, B. J., P. J. Neiman, F. M. Ralph, and F. E. Barthold, 2012: Physical processes associated with heavy flooding rainfall in Nashville, Tennessee, and vicinity during 12 May 2010: The role of an atmospheric river and mesoscale convective systems. *Mon. Wea. Rev.,* **140,** 358–378, doi:10.1175/MWR-D-11-00126.1.

Muller, C. J., and P. A. O'Gorman, 2011: An energetic perspective on the regional response of precipitation to climate change. *Nat. Climate Change,* **1,** 266–271, doi:10.1038/nclimate1169.

Neiman, P. J., F. M. Ralph, A. B. White, D. E. Kingsmill, and P. O. G. Persson, 2002: The statistical relationship between upslope flow and rainfall in California's coastal mountains: Observations during CALJET. *Mon. Wea. Rev.,* **130,** 1468–1492, doi:10.1175/1520-0493(2002)130<1468:TSRBUF>2.0.CO;2.

——, ——, G. A. Wick, Y.-H. Kuo, T.-K. Wee, Z. Ma, G. H. Taylor, and M. D. Dettinger, 2008a: Diagnosis of an intense atmospheric river impacting the Pacific Northwest: Storm summary and offshore vertical structure observed with COSMIC satellite retrievals. *Mon. Wea. Rev.,* **136,** 4398–4420, doi:10.1175/2008MWR2550.1.

——, ——, ——, J. D. Lundquist, and M. D. Dettinger, 2008b: Meteorological characteristics and overland precipitation impacts of atmospheric rivers affecting the west coast of North America based on eight years of SSM/I satellite observations. *J. Hydrometeor.,* **9,** 22–47, doi:10.1175/2007JHM855.1.

——, L. J. Schick, F. M. Ralph, M. Hughes, and G. A. Wick, 2011: Flooding in western Washington: The connection to atmospheric rivers. *J. Hydrometeor.,* **12,** 1337–1358, doi:10.1175/2011JHM1358.1.

O'Gorman, P. A., and T. Schneider, 2009: The physical basis for increases in precipitation extremes in simulations of 21st-century climate change. *Proc. Natl. Acad. Sci. USA,* **106,** 14 773–14 777, doi:10.1073/pnas.0907610106.

——, and C. J. Muller, 2010: How closely do changes in surface and column water vapor follow Clausius–Clapeyron scaling in climate change simulations? *Environ. Res. Lett.,* **5,** 025207, doi:10.1088/1748-9326/5/2/025207.

——, R. Allan, M. Byrne, and M. Previdi, 2012: Energetic constraints on precipitation under climate change. *Surv. Geophys.,* **33,** 585–608, doi:10.1007/s10712-011-9159-6.

Pall, P., M. Allen, and D. Stone, 2007: Testing the Clausius–Clapeyron constraint on changes in extreme precipitation under CO_2 warming. *Climate Dyn.,* **28,** 351–363, doi:10.1007/s00382-006-0180-2.

Pendergrass, A. G., and D. L. Hartmann, 2014: The atmospheric energy constraint on global-mean precipitation change. *J. Climate,* **27,** 757–768, doi:10.1175/JCLI-D-13-00163.1.

Ralph, F. M., P. J. Neiman, and G. A. Wick, 2004: Satellite and CALJET aircraft observations of atmospheric rivers over the eastern North Pacific Ocean during the winter of 1997/98. *Mon. Wea. Rev.,* **132,** 1721–1745, doi:10.1175/1520-0493(2004)132<1721:SACAOO>2.0.CO;2.

——, ——, and R. Rotunno, 2005: Dropsonde observations in low-level jets over the northeastern Pacific Ocean from CALJET-1998 and PACJET-2001: Mean vertical-profile and atmospheric-river characteristics. *Mon. Wea. Rev.,* **133,** 889–910, doi:10.1175/MWR2896.1.

——, ——, G. A. Wick, S. I. Gutman, M. D. Dettinger, D. R. Cayan, and A. B. White, 2006: Flooding on California's Russian River: Role of atmospheric rivers. *Geophys. Res. Lett.,* **33,** L13801, doi:10.1029/2006GL026689.

——, T. Coleman, P. J. Neiman, R. J. Zamora, and M. D. Dettinger, 2013: Observed impacts of duration and seasonality of atmospheric-river landfalls on soil moisture and runoff in coastal northern California. *J. Hydrometeor.,* **14,** 443–459, doi:10.1175/JHM-D-12-076.1.

Rutz, J. J., W. J. Steenburgh, and F. M. Ralph, 2014: Climatological characteristics of atmospheric rivers and their inland penetration over the western United States. *Mon. Wea. Rev.,* **142,** 905–921, doi:10.1175/MWR-D-13-00168.1.

Salathé, E. P., Jr., 2006: Influences of a shift in North Pacific storm tracks on western North American precipitation under global warming. *Geophys. Res. Lett.,* **33,** L19820, doi:10.1029/2006GL026882.

Scheff, J., and D. M. W. Frierson, 2012: Robust future precipitation declines in CMIP5 largely reflect the poleward expansion of model subtropical dry zones. *Geophys. Res. Lett.,* **39,** L18704, doi:10.1029/2012GL052910.

Singh, M. S., and P. A. O'Gorman, 2012: Upward shift of the atmospheric general circulation under global warming: Theory and simulations. *J. Climate,* **25,** 8259–8276, doi:10.1175/JCLI-D-11-00699.1.

Sodemann, H., and A. Stohl, 2013: Moisture origin and meridional transport in atmospheric rivers and their association with multiple cyclones. *Mon. Wea. Rev.,* **141,** 2850–2868, doi:10.1175/MWR-D-12-00256.1.

Stephens, G. L., and Coauthors, 2010: Dreary state of precipitation in global models. *J. Geophys. Res.,* **115,** D24211, doi:10.1029/2010JD014532.

——, and Coauthors, 2012: An update on earth's energy balance in light of the latest global observations. *Nat. Geosci.,* **5,** 691–696, doi:10.1038/ngeo1580.

Taylor, K. E., R. J. Stouffer, and G. A. Meehl, 2012: An overview of CMIP5 and the experiment design. *Bull. Amer. Meteor. Soc.,* **93,** 485–498, doi:10.1175/BAMS-D-11-00094.1.

Trenberth, K. E., 1999: Conceptual framework for changes of extremes of the hydrological cycle with climate change. *Weather and Climate Extremes,* T. Karl, N. Nicholls, and A. Ghazi, Eds., Springer, 327–339.

——, and C. J. Guillemot, 1998: Evaluation of the atmospheric moisture and hydrological cycle in the NCEP/NCAR reanalyses. *Climate Dyn.,* **14,** 213–231, doi:10.1007/s003820050219.

——, D. Aiguo, R. M. Rasmussen, and D. B. Parsons, 2003: The changing character of precipitation. *Bull. Amer. Meteor. Soc.,* **84,** 1205–1217, doi:10.1175/BAMS-84-9-1205.

——, L. Smith, Q. Taotao, D. Aiguo, and J. Fasullo, 2007: Estimates of the global water budget and its annual cycle using observational and model data. *J. Hydrometeor.,* **8,** 758–769, doi:10.1175/JHM600.1.

van Oldenborgh, G. J., M. Collins, J. Arblaster, J. H. Christensen, J. Marotzke, S. B. Power, M. Rummukainen, and T. Zhou, Eds., 2013: Annex I: Atlas of global and regional climate projections supplementary material RCP8.5. *Climate Change 2013: The Physical Science Basis,* T. F. Stocker et al., Eds., Cambridge University Press, AISM-1–AISM-159. [Available online at www.climatechange2013.org/images/report/WG1AR5_AISM8.5_FINAL.pdf.]

Viale, M., and M. N. Nunez, 2011: Climatology of winter orographic precipitation over the subtropical central Andes and associated synoptic and regional characteristics. *J. Hydrometeor.,* **12,** 481–507, doi:10.1175/2010JHM1284.1.

Warner, M. D., C. F. Mass, and E. P. Salathé, 2012: Wintertime extreme precipitation events along the Pacific Northwest coast: Climatology and synoptic evolution. *Mon. Wea. Rev.,* **140,** 2021–2043, doi:10.1175/MWR-D-11-00197.1.

Widmann, M., C. S. Bretherton, and E. P. Salathe, 2003: Statistical precipitation downscaling over the northwestern United States using numerically simulated precipitation as a predictor. *J. Climate,* **16,** 799–816, doi:10.1175/1520-0442(2003)016<0799:SPDOTN>2.0.CO;2.

Yin, J. H., 2005: A consistent poleward shift of the storm tracks in simulations of 21st century climate. *Geophys. Res. Lett.,* **32,** L18701, doi:10.1029/2005GL023684.

Zappa, G., L. C. Shaffrey, and K. I. Hodges, 2013: The ability of CMIP5 models to simulate North Atlantic extratropical cyclones. *J. Climate,* **26,** 5379–5396, doi:10.1175/JCLI-D-12-00501.1.

Zhu, Y., and R. E. Newell, 1998: A proposed algorithm for moisture fluxes from atmospheric rivers. *Mon. Wea. Rev.,* **126,** 725–735, doi:10.1175/1520-0493(1998)126<0725:APAFMF>2.0.CO;2.